ORIGINAL ARTICLE

Feasibility of ultra-high-speed acquisition in xSPECT bone algorithm: a phantom study with advanced bone SPECT-specific phantom

Hajime Ichikawa[1,2] · Noriaki Miyaji[3] · Masahisa Onoguchi[2] · Takayuki Shibutani[2] · Akio Nagaki[4] · Toyohiro Kato[1] · Hideki Shimada[1]

Abstract

Objective Although xSPECT Bone (xB) provides quantitative single-photon emission computed tomography (SPECT) high-resolution images, patients' burden remains high due to long acquisition time; therefore, this study aimed to investigate the feasibility of shortening the xB acquisition time using a custom-designed phantom.

Methods A custom-designed xSPECT bone-specific (xSB) phantom with simulated cortical and spongious bones was developed based on the thoracic bone phantom. Both standard- and ultra-high-speed (UHS) xB acquisitions were performed in a male patient with lung cancer. In this phantom study, SPECT was acquired for 3, 6, 9, 12, and 30 min. The clinical SPECT acquisition time per rotation was 9 and 3 min for standard and UHS, respectively. SPECT images were reconstructed using ordered subset expectation maximization with three-dimensional resolution recovery (Flash3D; F3D) and xB algorithms. Quantitative SPECT value (QSV) and coefficient of variation (CV) were measured using the volume of interests (VOIs) placed at the center of the vertebral body and hot sphere. A linear profile was plotted on the spinous process at the center of the xSB phantom; then, the full width at half maximum (FWHM) was measured. The standardized uptake value (SUV) and standard deviation from the first thoracic to the fifth lumbar vertebrae in clinical standard- and UHS-xB images were measured using a 1-cm^3 VOI.

Results The QSV of F3D images was underestimated even in large regions, whereas those of xB images were close to actual radioactivity concentration. The CV was similar or lower for xB images than that for F3D images but was not decreased with increasing acquisition time for both reconstruction images. The FWHM of xB images was lower than those of F3D images at all acquisition times. The mean SUV values from the first thoracic to fifth lumbar vertebrae for standard- and UHS-xB images were 6.73 ± 0.64 and 6.19 ± 0.87, respectively, showing a strong positive correlation.

Conclusions Results of this phantom study suggest that xB imaging can be obtained in only one-third of the acquisition time without compromising the image quality. The SUV of UHS-xB images can be similar to that of standard-xB images in terms of clinical interpretation.

Keywords Bone scintigraphy · Quantitative single-photon emission computed tomography (SPECT) · xSPECT bone · Phantom study

✉ Masahisa Onoguchi
onoguchi@staff.kanazawa-u.ac.jp

1 Department of Radiology, Toyohashi Municipal Hospital, 50 Aza Hachiken Nishi, Aotake–Cho, Toyohashi, Aichi 4418570, Japan

2 Department of Quantum Medical Technology, Graduate School of Medical Sciences, Kanazawa University, 5-11-80 Kodatsuno, Kanazawa, Ishikawa 9200942, Japan

3 Department of Nuclear Medicine, Cancer Institute Hospital of Japanese Foundation for Cancer Research, 3-8-31 Ariake, Koto-ku, Tokyo 1358550, Japan

4 Department of Radiological Technology, Kurashiki Central Hospital, 1-1-1 Miwa, Kurashiki, Okayama 7108602, Japan

Introduction

Bone scintigraphy has been widely used to diagnose bone metastases and non-oncologic bone diseases. Nowadays, hybrid imaging using single-photon emission computed tomography with computed tomography (SPECT/CT) is used and thereby able to also provide quantitative SPECT images [1–6]. Among them, xSPECT Bone (xB) is a new reconstruction algorithm using five tissue segmentation images called as zone map, which delineated tissue boundaries by CT images, resulting in high-resolution quantitative images [7–11]. The zone map is defined in five classes: the lung, adipose, soft tissue, spongious bone, and cortical bone.

Previous studies have revealed that SPECT/CT from the cervical spine to the pelvis can improve the diagnostic accuracy of bone metastases [12–14]; however, the scanning requires prolonged examination time, ~ 30 min, which increases the patient's burden. Zacho et al. [15] have reported that the addition of 3 min per bed SPECT/CT to the planar whole-body scan provides the same diagnostic performance as 11 min. However, although the report mentioned that the 3 min per bed SPECT/CT images were significantly less smooth, no assessment of image quality was performed. Shortening the acquisition time

is challenging in xB images since its matrix size is double that of a general SPECT image, resulting in increased noise levels under the same acquisition time. Furthermore, previous studies have demonstrated high image resolution and quantitative performance of xB images at acquisition times recommended by the manufacturer [11]; however, acquisition parameters of xB images have not been investigated due to the lack of optimal phantoms for xB image assessment.

Therefore, this study aimed to validate the feasibility of shortening the xB acquisition time. The potential impact of varying the acquisition time on the quantitative accuracy and image noise for xB images was assessed in custom-design phantom studies. Additionally, the standardized uptake value (SUV) and image noise of one patient with standard and short acquisition time was analyzed.

Materials and methods

Phantom design

The requirement for ethical review was waived by the medical ethics review committee of our hospital because of the nature of this study. We developed a custom-design xSPECT bone-specific (xSB) phantom based on the thoracic bone

Fig. 1 The custom-designed xSPECT bone-specific (xSB) phantom configured with vertebral body and spinous and transverse processes. **a** Frontal view; **b** transverse and **c** sagittal CT images of the phantom; and **d** Sagittal SPECT image of the phantom
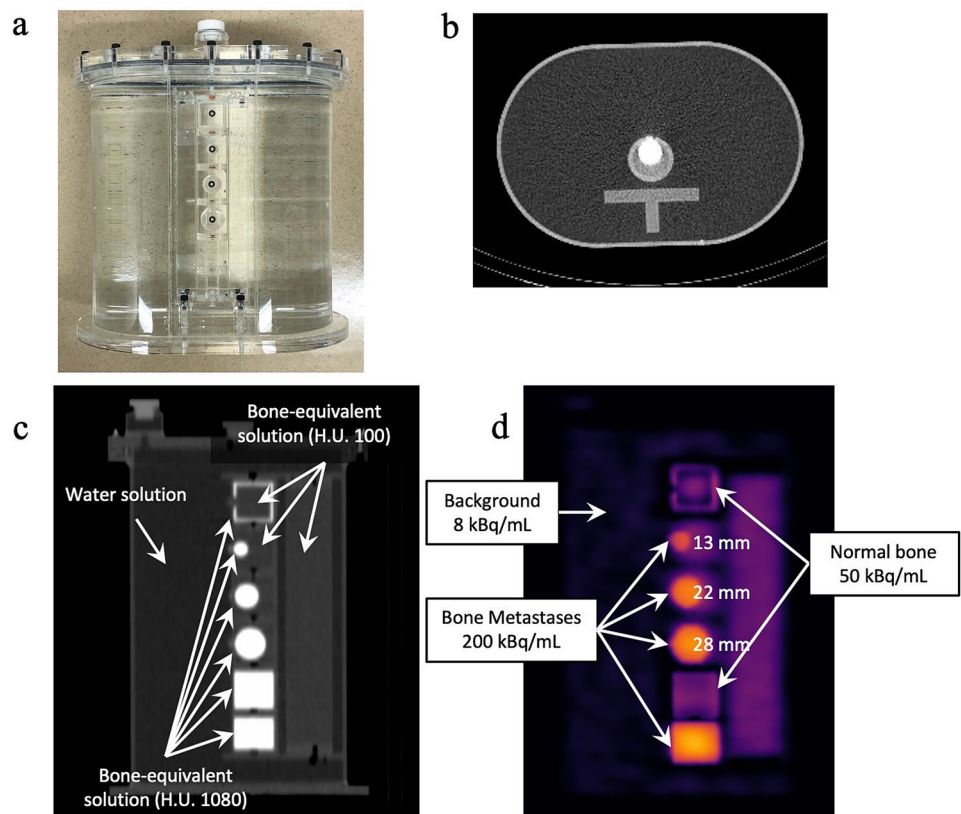
phantom (Fig. 1) [16]. A particular design of the phantom was simulated in the cortical and spongious bones of the zone map used in xB reconstruction algorithm. The vertebral body (including the cortical bone, spongious bone, and bone metastases) and the spinous and transverse processes contained a bone-equivalent solution of K_2HPO_4 and ^{99m}Tc [17]. The first vertebra was equipped with a 2-mm-thickness cortical bone (Hounsfield units; HU 1080–50 kBq/mL) and 28-mm-diameter and 27-mm-height spongious bone (HU 100–50 kBq/mL) [2]. The spherical lesions with diameters of 13, 22, and 28 mm were inserted in the second, third, and fourth vertebral body, respectively (HU 1080–200 kBq/mL). The fifth and sixth vertebrae were the reference sections for the normal (HU 1080–50 kBq/mL) and tumor bone activity concentrations (HU 1080–200 kBq/mL), respectively.

The patient

We present the case of a male patient with lung cancer who underwent bone scintigraphy. His pain exacerbated 3 months after bone scintigraphy; therefore, repeat bone scintigraphy was performed. At the second bone scintigraphy, the patient complained of strong pain, which prevented a prolonged scanning time due to routine xB protocol. On both occasions, the torso SPECT/CT scan was immediately acquired after a whole-body planar scan at 2.5 h after injecting ^{99m}Tc-hydroxymethylenediphosphonate activity of 740 MBq. Due to the retrospective study design, informed consent was obtained from this subject in the form of opt-out.

SPECT/CT data acquisition and reconstruction

All images were acquired using a Symbia Intevo 2 hybrid SPECT/CT system, equipped with a low-energy high-resolution collimator (Siemens Healthcare, Erlangen, Germany). SPECT acquisitions were performed using the following parameters: energy window, 15% at 140 keV; lower subwindow, 15% for scatter correction; 256×256 matrix and 1.0-zoom (with a 2.4×2.4 mm^2 pixel); 120 views over 360 °; and continuous mode through the elliptical orbit. For phantom studies, SPECT images were acquired for 3, 6, 9, and 12 min. The SPECT image that was acquired for 30 min was used as a reference. Clinical data were also acquired with the SPECT/CT system using the same parameters as in the phantom studies, except for the acquisition time. Acquisition times of SPECT per rotation were 9 min and 3 min for the first (standard; std) and second (ultra-high-speed; UHS) times, respectively.

CT scanning at 130 kV was performed on a 2.0-mm thick slice, with dose modulation and quality reference of 40 mAs, pitch 2. CT data were reconstructed using kernels of H08 SPECT AC for F3D and H31 for xB.

We reconstructed the SPECT images using the following algorithms: ordered subset expectation maximization with three-dimensional resolution recovery (Flash3D; F3D) and xB, both with manufacturer-specific parameters. F3D reconstructions were performed with subsets two, iteration 24, and 10-mm Gaussian filter after converting the matrix size to 128×128, a common matrix size for SPECT. In phantom studies, to convert SPECT count density to quantitative SPECT, cylindrical phantom of 22 cm in diameter and 22 cm in height (Kyoto Kagaku, Kyoto, Japan) filled with ^{99m}Tc solution of known radioactivity concentration was used to determine a cross-calibration factor (CCF) using the GI-BONE software (Nihon Medi-Physics, Tokyo, Japan) [18]. A dose calibrator (CRC-55tW; Capintec, Ramsey, MN, USA) for cross-calibration, calibrated with a standard reference ^{137}Cs source (the measurement error by the manufacturer was -1.3%), was used. The actual quantitative SPECT value (QSV) for the phantom and SUV for the patient were calculated as.

QSV (Bq/mL) = CCF (Bq/cps) × count density (cps/mL).
SUV = QSV × Body weight (g) / Injected dose (Bq).

Reconstruction parameters for xB were automatically optimized using the xRecon program (version VB20; Siemens Healthcare, Erlangen, Germany) for the number of iterations and the size of the full width at half maximum (FWHM) of the Gaussian filter depending on counts of projection data (subsets were fixed at one). Consequently, the parameters shown in Table 1 were assigned. In the xRecon program, xB images were reconstructed and converted to QSVs using system planar sensitivity with a ^{99m}Tc point source [7]. The parameters for the clinical data were also identically adapted to the phantom conditions.

Data analysis

Phantom studies

The quantitative accuracy of xSB phantom images was evaluated on the basis of QSVs, and the image noise was estimated based on the percentage of coefficient of variations (%CV). QSVs (Bq/mL) were measured using the volume

Table 1 Reconstruction parameters of xSPECT bone for various acquisition times

Acq. time (min.)	Subset	Iterations	Gaussian filter (mm)
3	1	24	13
6	1	24	13
9	1	48	10
12	1	48	10
30	1	72	10

of interests (VOIs), which was placed at the center of the vertebrae and hot spheres. The means and standard deviations (SDs) within VOIs were obtained, and %CV was calculated as SDs divided by the mean. QSVs in the first, fifth, and sixth vertebrae and 13-, 22-, and 28-mm hot spheres of the xSB phantom images were measured with VOI setting using the GI-BONE software. The actual activity concentration in the xSB phantom was measured using a well counter (CAPRAC-t; Capintec, Ramsey, MN, USA) and decay correction. The line profile was drawn on the central slice of the first lumbar vertebra in the QSV image, and the radioactivity concentration distribution was assessed. Additionally, spatial resolution was assessed using the line spread function of the spinous process. The line profile was plotted on the spinous process using 10 slices at the center of the xSB phantom, and FWHM was calculated as the mean of ten slices.

Clinical cases for std- and UHS-xB

Spherical VOIs of 1 cm^3 were set as a reference to CT images of the bone window to measure SUVs and SDs from the first thoracic to the fifth lumbar vertebrae in clinical xB images using the Syngo Via software (Siemens Healthcare, Erlangen, Germany). Each of the 17 spherical VOIs was set at the center of the vertebral body as much as possible without abnormal accumulation and degenerative changes. The FWHM was also measured by drawing a profile curve on the spinous process of the fifth lumbar vertebra.

Statistical analysis

The Friedman test was used to analyze the impact of acquisition time on QSVs and %CV. The QSVs in the F3D and xB images were compared using Wilcoxon signed-rank tests after evaluating the non-normal distribution using Shapiro–Wilk tests. Correlations between the SUVs of std-xB and UHS-xB were analyzed using Pearson's correlation coefficients. Differences in SDs of std-xB and UHS-xB were analyzed using paired t tests. A p value of <0.05 was considered significant. All data were statistically analyzed using the IBM SPSS statistics version 27 (IBM Corp., Armonk, NY, USA).

Results

Phantom studies

Figure 2 presents F3D and xB images at each acquisition time. The 13-mm sphere and intervertebral space were observable in xB but were undetectable in F3D. The noise and background of the spinous process were improved by increasing the acquisition time in F3D images. Radioactivity concentrations of the cortical and spongious bones in the first vertebra were almost similar, whereas those of the cortical bone with high HU were decidedly higher than those of the spongious bone in xB images. In F3D image, the highest value was observed at the center of the homogeneous
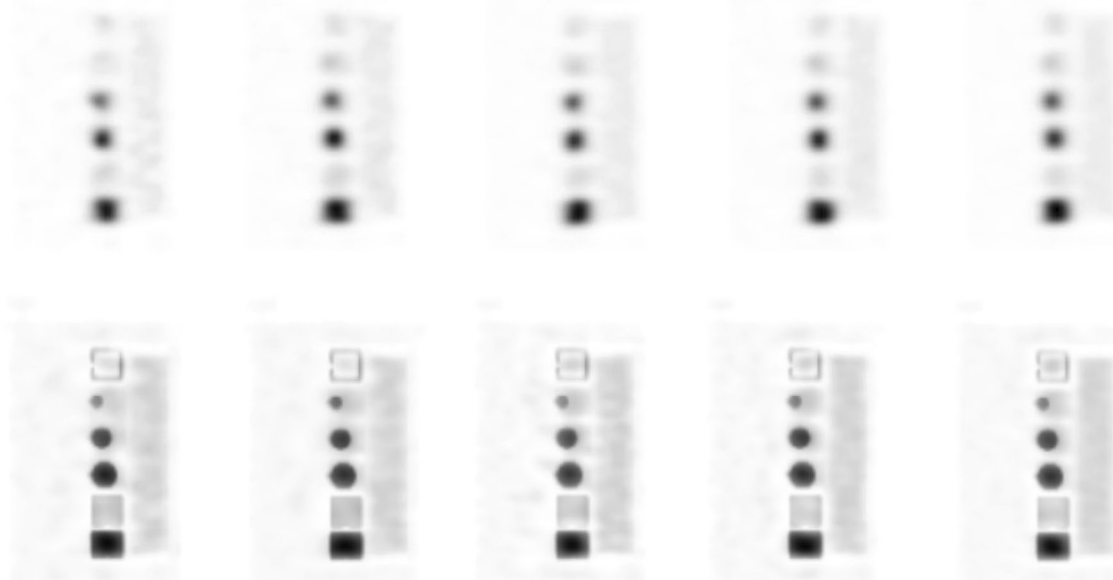
Fig. 2 Sagittal image of the custom-designed xSPECT bone-specific (xSB) phantom. Flash3D images (top row) and xSPECT bone images (bottom row). The acquisition times are 3, 6, 9, 12, and 30 min from left to right

accumulation; however, in the xB images, the border of the fifth vertebra revealed a higher density than the center. The impact of acquisition time was not visually observed for xB images.

QSVs of both F3D and xB images were independent of the acquisition time (Fig. 3a, b), which were significantly higher in xB images than those in F3D images in regions other than the first vertebra. The QSVs of F3D were significantly underestimated even for the relatively larger regions of the first, fifth, and sixth vertebrae. However, the QSVs of xB images were similar to the true values, except for the underestimation in the first vertebra covered by the cortical bone and the small region of the 13-mm sphere. The %CV revealed similar or lower values of xB than F3D, except that xB was higher in the 13-mm sphere (Fig. 3c, d). No reduction in %CV was observed with prolonged acquisition time for either reconstruction method.

The profile curves of the first lumbar vertebra in F3D and xB images for each acquisition time are illustrated in Fig. 4. The F3D image was underestimated, whereas the xB image was overestimated, especially at both boundaries.

The FWHM of the spinous process in F3D images was 19.4 ± 1.2, 18.8 ± 1.1, 18.0 ± 0.7, 17.4 ± 0.8, and 17.7 ± 0.5 mm at 3-, 6-, 9-, 12-, and 30-min acquisition times, respectively. Similarly, the FWHM of xB images was 14.3 ± 0.8, 15.7 ± 0.7, 13.5 ± 0.8, 12.8 ± 0.2, and 12.6 ± 0.2 mm at 3-, 6-, 9-, 12-, and 30-min acquisition times, respectively. The FWHM of xB was lower than that of F3D at all acquisition times; moreover, the FWHM decreased with increasing acquisition time and exhibited almost the same value at 12 and 30 min for both reconstruction methods.

Fig. 3 Radioactivity concentration (**a**, **b**) and % coefficient of variation (**c**, **d**) for two reconstruction methods at various acquisition times. No significant differences were found in the Friedman test
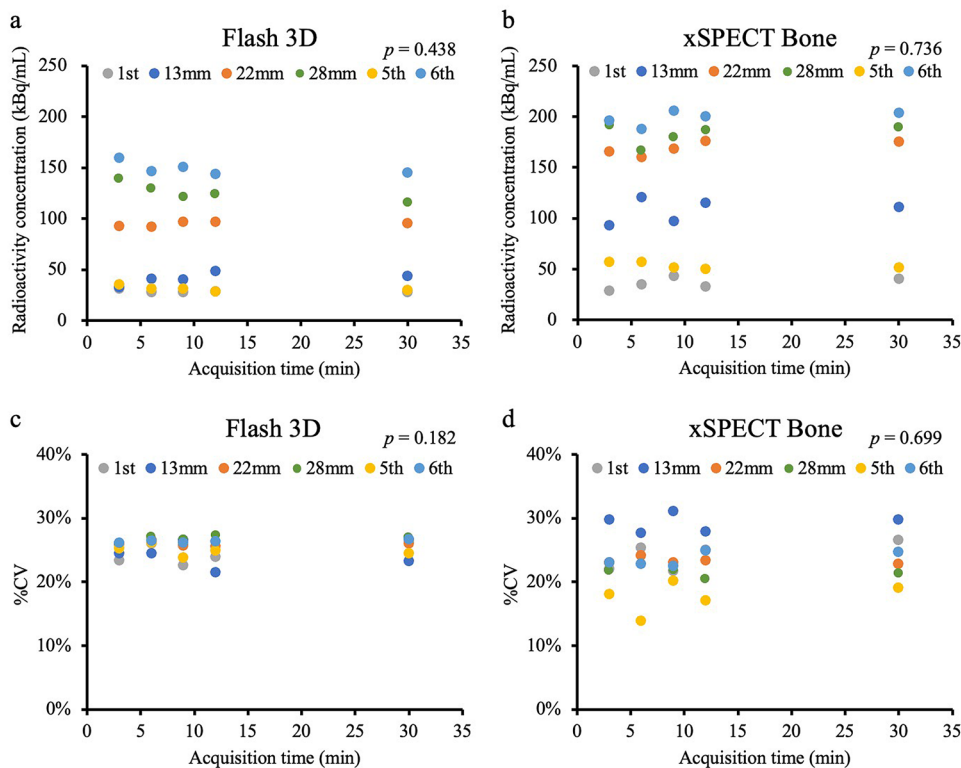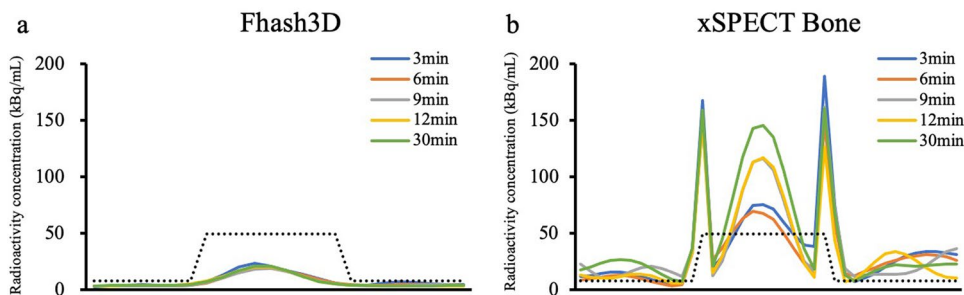

Fig. 4 Measured profiles of the first lumbar vertebra at various acquisition times for Flash3D (**a**) and xSPECT bone (**b**). The dashed line shows the actual radioactivity concentration

Clinical cases for std- and UHS-xB

Abnormal accumulation in the left fifth rib, left iliac, and left lesser trochanter of the femur, and degenerative changes in the right first rib, sixth, and seventh thoracic vertebrae and the third and fourth lumbar vertebrae are revealed on std-xB and UHS-xB images (Fig. 5). The nuclear medicine physician interpreted the second bone scintigraphy, including whole-body planar images, general SPECT/CT images, and xB images, as increased accumulation due to bone metastases in the left iliac bone and left fifth rib, decreased accumulation in the right greater tubercle of the humerus, and unchanged degenerative changes in the thoracic and lumbar spine as compared with the first. The mean SUVs in the first thoracic to fifth lumbar vertebrae without any abnormal accumulation and degenerative changes for std-xB and UHS-xB images were 6.73 ± 0.64 and 6.19 ± 0.87, respectively. With $r = 0.845$, a strong positive correlation was observed in the results (Fig. 6). The mean SDs in the first thoracic to fifth lumbar vertebrae for std-xB and UHS-xB were 0.90 ± 0.26 and 0.66 ± 0.21, respectively, which were significantly lower for UHS-xB than for std-xB. The FWHM of the fifth lumbar vertebra in the std-xB and UHS-xB images were 10.3 mm and 10.8 mm, respectively.
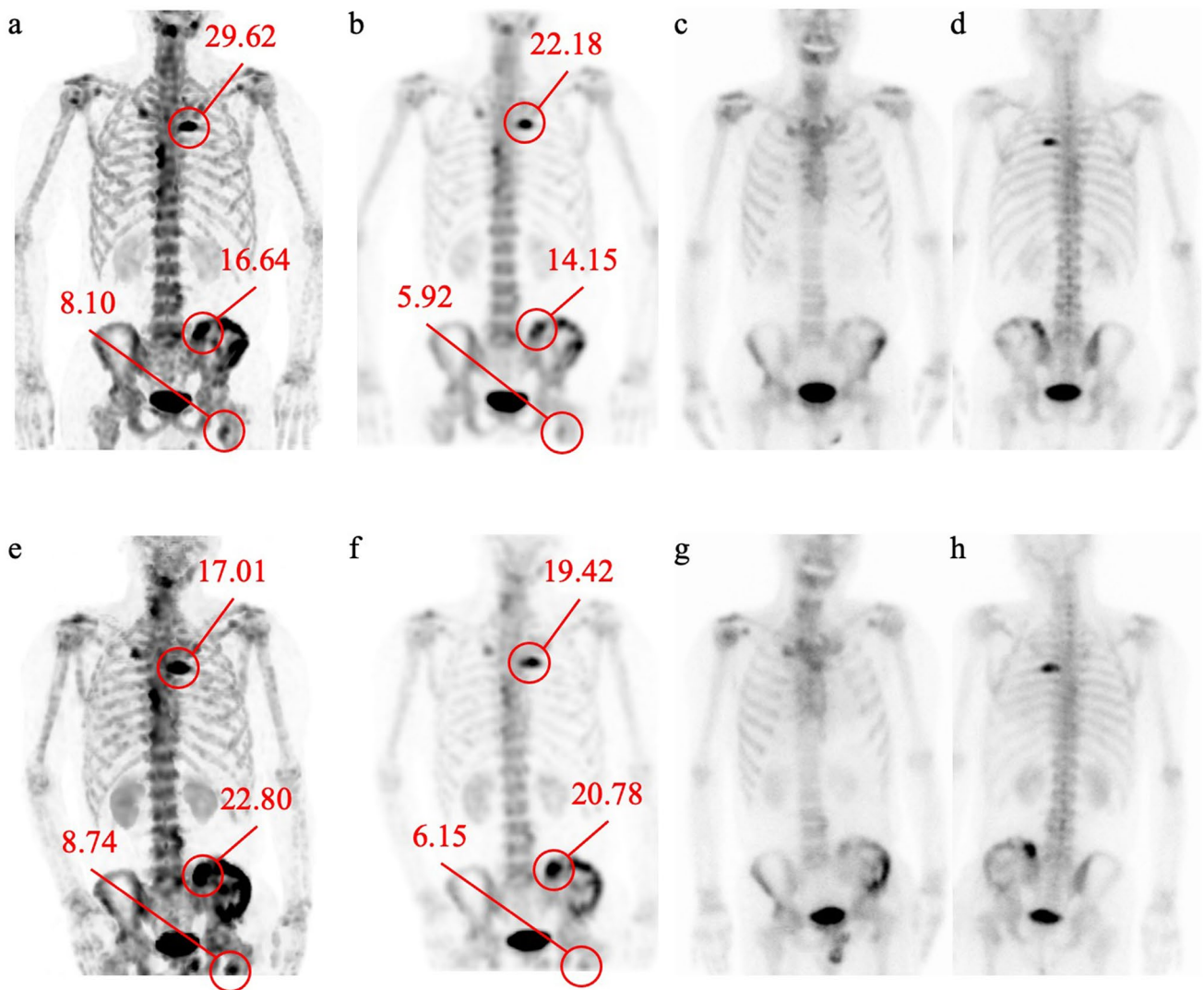

Fig. 5 Clinical images are shown from left to right; maximum intensity projections (MIP) images of xSPECT bone (**a**, **e**), MIP images of Flash3D (**b**, **f**), anterior (**c**, **g**), and posterior (**d**, **h**) whole-body planar images. Upper row: standard acquisition time; lower row: ultra-high-speed acquisition time (the acquisition time of whole-body planar images is equal). Numerical values noted for reference indicate the standardized uptake value (SUV)
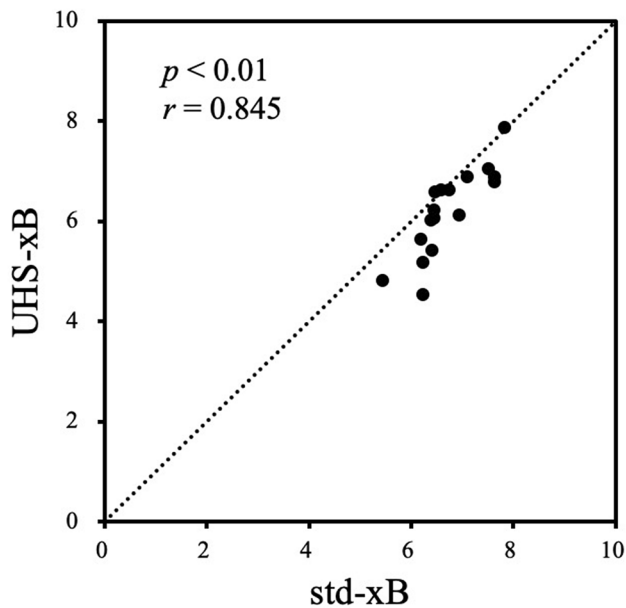
Fig. 6 Correlation of SUV between the standard and ultra-high-speed xSPECT bone images from the first thoracic to the fifth lumbar vertebrae

Discussion

Our study investigated the feasibility of adapting a UHS protocol for xB acquisition using the xSB phantom. In the phantom study, visual impression, QSV, and %CV did not significantly differ depending on the acquisition time for both F3D and xB images. However, xB images revealed significantly superior performance than F3D images, especially in the 13-mm sphere. Remarkably, UHS-xB images revealed superior noise characteristics than std-xB images.

xB images showed no significant impact on QSV and %CV under the acquisition times available in clinical practice even in 3 min. Previous studies on SPECT/CT have reported that F3D images with the 3-min acquisition are comparable to those with 11-min in terms of diagnostic performance [15]. Additionally, another study has revealed that xB images have higher resolution and quantitative accuracy than F3D images [11]. xB images with doubled matrix size than F3D requires an eightfold increase in acquisition time to obtain the same noise level. Nevertheless, the %CVs of xB were superior to those of F3D, except for the 13-mm sphere. The superior %CV of F3D for the 13-mm sphere was probably because the sphere was not ever detected owing to low-resolution characteristics with F3D. The 13-mm sphere cannot be detected in F3D images [19]. This is probably because the reconstruction algorithm of xB is completely different from that of F3D, and reconstruction parameters are optimized according to the count density [7]. Due to the slight accumulation of the left femoral lesser trochanter,

SUVs of std- and UHS-xB images were higher than those of std- and UHS-F3D images (Fig. 5). Considering that the SUV of the normal bone is 6.2–7.0 as the threshold level [3, 5], the accumulation interpretation may differ between F3D and xB images. The most important factor in bone scintigraphy images is the ability to detect smaller or lower-contrast accumulations, although the quantitative accuracy in SPECT images and noise characteristics are also important. The 13-mm sphere in the phantom image is observed in xB images, and the accumulation in the lesser trochanter of the femur in clinical images is more clearly interpreted than in F3D or whole-body images even in the UHS-xB image. However, the cortical bone in the first vertebra of xSB phantom images was over-accumulated, which may be a specific characteristic of the xB algorithm, creating a zone map based on the HU and estimates the count distribution for individual zones, as shown in our xSB phantom study. The xB image may overestimate the accumulation with high HU, such as degenerative changes, and the hyperostosis of the vertebral body was also clearly accumulated on xB clinical images [9, 20]. Although this is not clinically significant, determining the distribution accuracy of radiopharmaceuticals or an artifact specific to xB algorithm is difficult; therefore, the validation of the algorithm and optimization of acquisition and/or reconstruction parameters using a specific phantom are important.

Using the xSB phantom in this study would be more suitable to validate xB algorithm than previous studies using other phantoms. Miyaji et al. reported the optimization of xB reconstruction parameters using a custom-design phantom for bone SPECT evaluation and bone-equivalent radioactive solution [11]. The report concludes that the optimized parameter for xB reconstruction is one subset of 48 iterations with a 6-mm Gaussian filter in their phantom studies. Our results demonstrated that almost similar reconstruction parameters were used for the 12-min acquisition data. However, the acquisition of xB images from the cervical spine to the pelvis requires a prolonged acquisition time of > 30 min; hence, it should be shortened as much as possible. Furthermore, no previous studies have evaluated phantom, and even if they did, due to the use of a specific concentration of a bone-equivalent solution, the artifact of over-accumulation with high HU was not clarified.

Although xB reconstruction, which automatically adjusts iterations and the FWHM of the Gaussian filter according to the total counts, was maintained at the %CV constant independent of the total counts, it might still be considered a problem in maintaining the quantification accuracy [21]. Particularly, image reconstruction parameters strongly affect smaller accumulations. Shortening the acquisition time slightly degrades the image resolution in xB images. However, image resolution and quantification of xB images are much better than those of F3D images acquired with

sufficient acquisition time. In clinical images, SUV tended to be higher in std-xB than in UFS-xB, although whether this was due to factors other than acquisition time and reconstruction parameters cannot be determined since the examination period was different. Further optimization of UFS-xB reconstruction parameters may lead to better harmonization with the SUV of std-xB in the future. This study will be a useful step to investigate the acquisition parameters of xB.

This study is limited because we used the number of iterations and the FWHM of the Gaussian filter, which is automatically adjusted according to the total count as recommended by the manufacturer during image reconstruction. No harmonized SUV may be obtained without fixed image reconstruction parameters for quantitative SPECT images. Additionally, since our study was designed for osteogenic bone metastases, osteolytic bone metastases were not investigated. In the future, more clinical xB images should be obtained in further studies.

Conclusions

Our results suggest that xB imaging can be acquired in one-third of the scan time without compromising the image quality based on the xSB phantom data. Compared to the standard acquisition time, the SUV of UHS-xB images may be greatly similar in terms of clinical outcomes.

References

1. Zeintl J, Vija AH, Yahil A, Hornegger J, Kuwert T. Quantitative accuracy of clinical 99mTc SPECT/CT using ordered-subset expectation maximization with 3-dimensional resolution recovery, attenuation, and scatter correction. J Nucl Med. 2010;51(6):921–8.
2. Cachovan M, Vija AH, Hornegger J, Kuwert T. Quantification of (99m)Tc-DPD concentration in the lumbar spine with SPECT/CT. EJNMMI Res. 2013;3:45.
3. Kaneta T, Ogawa M, Daisaki H, Nawata S, Yoshida K, Inoue T. SUV measurement of normal vertebrae using SPECT/CT with Tc-99m methylene diphosphonate. Am J Nucl Med Mol Imaging. 2016;6(5):262–8.
4. Kuji I, Yamane T, Seto A, Yasumizu Y, Shirotake S, Oyama M. Skeletal standardized uptake values obtained by quantitative SPECT/CT as an osteoblastic biomarker for the discrimination of active bone metastasis in prostate cancer. Eur J Hybrid Imaging. 2017;1(1):2.
5. Umeda T, Koizumi M, Fukai S, Miyaji N, Motegi K, Nakazawa S, et al. Evaluation of bone metastatic burden by bone SPECT/CT in metastatic prostate cancer patients: defining threshold value for total bone uptake and assessment in radium-223 treated patients. Ann Nucl Med. 2018;32(2):105–13.
6. Tabotta F, Jreige M, Schaefer N, Becce F, Prior JO, Nicod LM. Quantitative bone SPECT/CT: high specificity for identification of prostate cancer bone metastases. BMC Musculoskelet Disord. 2019;20(1):619.
7. Vija AH (2014) Introduction to xSPECT technology: evolving multimodal SPECT to become context-based and quantitative. Molecular

8. Imaging White Paper: Siemens Medical Solutions USA, Inc, Molecular Imaging
9. Armstrong IS, Hoffmann SA. Activity concentration measurements using a conjugate gradient (Siemens xSPECT) reconstruction algorithm in SPECT/CT. Nucl Med Commun. 2016;37(11):1212–7.
9. Duncan I, Ingold N. The clinical value of xSPECT/CT Bone versus SPECT/CT. A prospective comparison of 200 scans. Eur J Hybrid Imaging. 2018;2(1):4.
10. De Laroche R, Simon E, Suignard N, Williams T, Henry MP, Robin P, et al. Clinical interest of quantitative bone SPECT-CT in the preoperative assessment of knee osteoarthritis. Medicine. 2018;97(35):e11943.
11. Miyaji N, Miwa K, Tokiwa A, Ichikawa H, Terauchi T, Koizumi M, et al. Phantom and clinical evaluation of bone SPECT/CT image reconstruction with xSPECT algorithm. EJNMMI Res. 2020;10(1):71.
12. Palmedo H, Marx C, Ebert A, Kreft B, Ko Y, Turler A, et al. Whole-body SPECT/CT for bone scintigraphy: diagnostic value and effect on patient management in oncological patients. Eur J Nucl Med Mol Imaging. 2014;41(1):59–67.
13. Rager O, Nkoulou R, Exquis N, Garibotto V, Tabouret-Viaud C, Zaidi H, et al. Whole-body SPECT/CT versus planar bone scan with targeted SPECT/CT for metastatic workup. Biomed Res Int. 2017;2017:7039406.
14. Lofgren J, Mortensen J, Rasmussen SH, Madsen C, Loft A, Hansen AE, et al. A prospective study comparing 99mTc-hydroxyethylene-diphosphonate planar bone scintigraphy and whole-body SPECT/CT with 18F-fluoride PET/CT and 18F-fluoride PET/MRI for diagnosing bone metastases. J Nucl Med. 2017;58(11):1778–85.
15. Zacho HD, Manresa JAB, Aleksyniene R, Ejlersen JA, Fledelius J, Bertelsen H, et al. Three-minute SPECT/CT is sufficient for the assessment of bone metastasis as add-on to planar bone scintigraphy: prospective head-to-head comparison to 11-min SPECT/CT. EJNMMI Res. 2017;7(1):1.
16. Ichikawa H, Kato T, Shimada H, Watanabe Y, Miwa K, Matsutomo N, et al. Detectability of thoracic bone scintigraphy evaluated using a novel custom-designed phantom. Jpn J Nucl Med Technol. 2017;37(3):229–38.
17. Dreuille OD, Strijckmans V, Ameida P, Loc'h C, Bendriem B. Bone equivalent liquid solution to assess accuracy of transmission measurements in SPECT and PET. IEEE Trans Nucl Sci. 1997;44(3):1186–90.
18. Nakahara T, Daisaki H, Yamamoto Y, Iimori T, Miyagawa K, Okamoto T, et al. Use of a digital phantom developed by QIBA for harmonizing SUVs obtained from the state-of-the-art SPECT/CT systems: a multicenter study. EJNMMI Res. 2017;7(1):53.
19. Ichikawa H, Kawakami K, Onoguchi M, Shibutani T, Nagatake K, Hosoya T, et al. Automatic quantification package (Hone Graph) for phantom-based image quality assessment in bone SPECT: computerized automatic classification of detectability. Ann Nucl Med. 2021;35(8):937–46.
20. Delcroix O, Robin P, Gouillou M, Le Duc-Pennec A, Alavi Z, Le Roux PY, et al. A new SPECT/CT reconstruction algorithm: reliability and accuracy in clinical routine for non-oncologic bone diseases. EJNMMI Res. 2018;8(1):14.
21. Lasnon C, Desmonts C, Quak E, Gervais R, Do P, Dubos-Arvis C, et al. Harmonizing SUVs in multicentre trials when using different generation PET systems: prospective validation in non-small cell lung cancer patients. Eur J Nucl Med Mol Imaging. 2013;40(7):985–96.